Evaluation of Credibility and Limitations of the Non-Rigid Registration of Micro-CT Images as a Tool for Local Strain Analysis

G. Pyka[1], E. Van de Casteele[1], M. Depypere[2], G. Kerckhofs[1,3], J. Schrooten[1], F. Maes[2], and M Wevers[1]

[1]Department of Metallurgy and Materials Engineering, KU Leuven, Kasteelpark Arenberg 44 PB2450, B-3001 Leuven, Belgium
[2]ESAT - PSI, iMINDS - MIC Medical Image Computing, UZ Herestraat 49 - box 7003, 3000 Leuven, Belgium
[3]Biomechanics Research Unit, Université de Liège, B-4000 Liège, Belgium

Aims

Three dimensional (3D) porous structures exhibit very good mechanical properties and an attractive strength-to-weight ratio. Because of their high load bearing capabilities and outstanding energy absorption properties in combination with their lightweight, they are excellent engineering materials, which are nowadays often used in automobiles and aircrafts [1-2]. Beside their dependency on the composition and the microstructure of the raw material, the mechanical properties of porous structures also depend on the geometrical and morphological properties of the basic cell architecture [1, 2]. Therefore, the qualitative assessment of the local, actual 3D internal deformation occurring at the microscopic scale combined with a thorough morphological characterization is very important in order to understand the mechanical behaviour and capabilities of porous structures.

Several studies on the relationship between morphology and mechanical behaviour of various porous structures have been performed using an experimental image based technique, namely digital volume correlation (DVC) [3, 4]. DVC based analysis of µCT images acquired at different loading steps, allowed to evaluate the deformation and failure mechanisms of 3D structures, but also to calculate the local 3D strain across the entire volume of an object [5, 6]. With DVC the displacement fields are retrieved by tracking the same subvolume in the reference and deformed image volume. However, this approach assumes a linear similarity of the intensity patterns of the matching blocks. It requires, thus, an additional regularization or smoothing of the deformation field in order to compensate for the errors and noise in the estimated deformations.

A more robust technique based on automated non-rigid image registration was proposed in Ref. [7] which eliminates the limitations of current DVC approaches. In this approach the image registration is computed based on maximization of mutual information (MMI) [8] between the µCT data sets acquired at different loading conditions, which is more general and potentially more robust as no specific intensity relationship is assumed. However, the accuracy of this novel approach still needs to be proven. Therefore, this study focuses on further development and evaluation of the credibility of the non-rigid registration of micro-CT images as a tool for local strain analysis. The potential and limitations of the proposed approach was assessed, based on the simulated deformation of a phantom object. Additionally, a proof-of-concept case study was performed to investigate the correspondence between the local strain computations and the real deformation of in-situ loaded Ti6Al4V open porous structures manufactured by selective laser melting (SLM).

Materials

Ti6Al4V porous structures

In this study, Ti6Al4V porous structures produced by SLM starting from Ti6Al4V powder [Concept Laser GmbH, Germany] were investigated [9]. CAD models were created using Magics software [Materialise NV, Haasrode, Belgium] having an open porous unit cell and a designed height and diameter of 6 mm. The samples were manufactured with a designed beam thickness of 100 µm and pore thickness of 1 mm.

Methods

Non-rigid image registration

The images registration was performed using the Elastix software [10]. In the first step of the registration process, the data sets of the non-deformed and deformed object were registered using an Euler transform in order to correct any rigid movement. In the second step, a non-rigid deformation with a B-spline transform was computed. The registration procedure uses the adaptive stochastic gradient descent method to optimize the advanced mattes mutual information criterion between the two images [11].

Credibility analysis of the strain measurements

In order to evaluate the credibility of the strain measurements, simulated experiments were performed with a controlled deformation of an artificially created cross-shaped phantom object with a distinct gray scale pattern (Figure 1a), further referred to as cross-phantom.

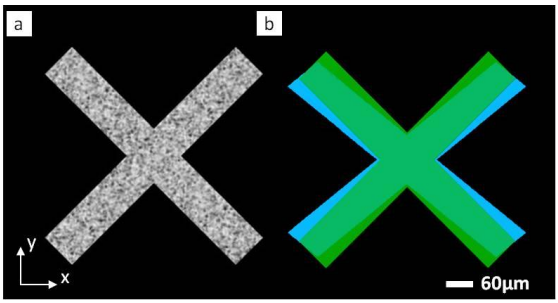

Figure 1. A typical cross-sectional image of the cross-phantom with distinct gray scale pattern (a) and the schematic visualization of the original (green) and deformed (blue) cross-phantom with applied 10% shrink and 10% stretch in y- and x-direction respectively (b).

The cross-phantom was extracted from a 2D image with a Gaussian random gray scale pattern and pasted in an empty 2D image with a black background. The 2D image with the textured cross was subsequently used to build the 3D data set with dimension 593x593x100 µm in x, y and z direction respectively. The isotropic voxel size was set to 1 µm and the thickness of the cross arms was 60 µm. In the shrink-stretch test, the image with the cross-phantom (Figure 1a) was shrunk in the y-direction by about 10% and stretched in the x-direction also by about 10% (Figure 1b). The normal strains ε_x, ε_y ε_z in principal directions were calculated and the influence of the grid spacing (GS: 30, 60, 120 and 180 µm) of the B-spline lattice on the obtained strain results was evaluated.

Validation of the image registration

The precision of the non-rigid image registration process of µCT images, acquired during the in-situ compression of the Ti6AlV scaffolds, was assessed qualitatively by visual observation of the registered µCT images and quantitatively by matching the back-deformed CT data set

(µCT images generated after non-rigid image registration of the compressed sample) with the µCT images of the reference scan (non-compressed sample). Using the CTAn software (Bruker CT, Belgium) the non-deformed images of the porous structure were used as a region of interest (ROI) for the back-deformed data set. Voxels representing the porous structure within this ROI are then positively matched, while voxels representing air within the ROI are negatively matched. To evaluate the influence of the grid spacing parameter on the image registration precision, the registration was performed for the sample compressed until the UCS, applying a grid spacing range from 100 to 800 µm.

Local strain analysis of Ti6Al4V porous structures – case study

To evaluate the local volumetric strain in function of the applied displacement, the samples were compressed stepwise, using an in house made micro-mechanical compression setup, at a constant rate of 0.2 mm/min, followed by µCT scanning. First, a pre-load of 0.01 kN was applied (step-0) and then a reference scan of the non-compressed sample was performed. In the first (step-1) and second (step-2) compression step the samples were compressed up to a displacement corresponding to 50% of the ultimate compressive strain (50%UCS) and the UCS, respectively, followed by µCT scanning. Additionally, the samples were further compressed up to a point in which the scaffolds beams started to collapse (step-3). The latter was obtained at the compression step corresponding to 8% of the absolute compressive strain applied to the samples. After each of the three compression steps, the micro-compression setup was placed in the nano-focus CT scanner (Phoenix NanoTom S GE Measurement and Control Solutions, Germany) and a 3D CT scan was performed according to the protocol presented in [9]. The radiographs were reconstructed using Phoenix datos|x 2.0 reconstruction software, resulting in images with an isotropic voxel size of 6.5 µm. 3D visualizations of the Ti6Al4V structures were generated using CTvox software (Bruker CT, Belgium).

Results

Cross-phantom test

Figure 2 presents the 2D and 3D visualization of the ε_x and ε_y strain computed with GS 30, 60, 120 and 180 µm, for the cross-phantom object during the shrink (10% in y-direction) and stretch (10% in x-direction) test of the cross-phantom. It can be observed that in the y-direction compressive strain was calculated and in the x-direction tensile strain. This corresponds well to the deformation (shrink and stretch in y-direction and x-direction, respectively) applied artificially to the image of the tested object. However, a strong influence of the GS on the strain analysis was also observed. Visually, the best results were obtained with GS 60 and 120 µm, which showed a more uniform distribution of the strain in both x- and y-directions (Figure 2). In case of GS 30 µm an overall inhomogeneity of the strain distribution was observed with local strain concentrations at the cross edges and corners. GS 180 µm resulted in a gradual decrease in the strain observed at the cross edges and corners located at the farthest distance from each other.

The strain distribution histograms, presented in Figure 3a, confirm quantitatively a diverse effect of the GS on the strain distribution. The largest strain distribution was observed with GS 30 µm (5% and 6.6% error for ε_x and ε_y strain, respectively) and 180 µm (5% and 3.5% error for ε_x and ε_y strain, respectively) while the GS 60 µm resulted in the most homogenous strain distribution in both x- and y-direction (1.3% and 0.9% error for ε_x and ε_y strain, respectively).

The mean and mode strain values were less sensitive to the GS and for all GS values around 10% compressive and tensile strain was calculated in the y- and x-direction, respectively, what corresponds to the artificially applied 10% deformation of the original image. The smallest deviation of the mean and mode strain (0.15% and 0.09% error for ε_x strain and 0.08% and 0.05% error for ε_y strain, respectively) was obtained with GS 120 µm. The largest deviation in

the strain level was observed with GS 180 µm as the mean strain in the x- and y-direction was 0.71% and 0.48%, respectively.

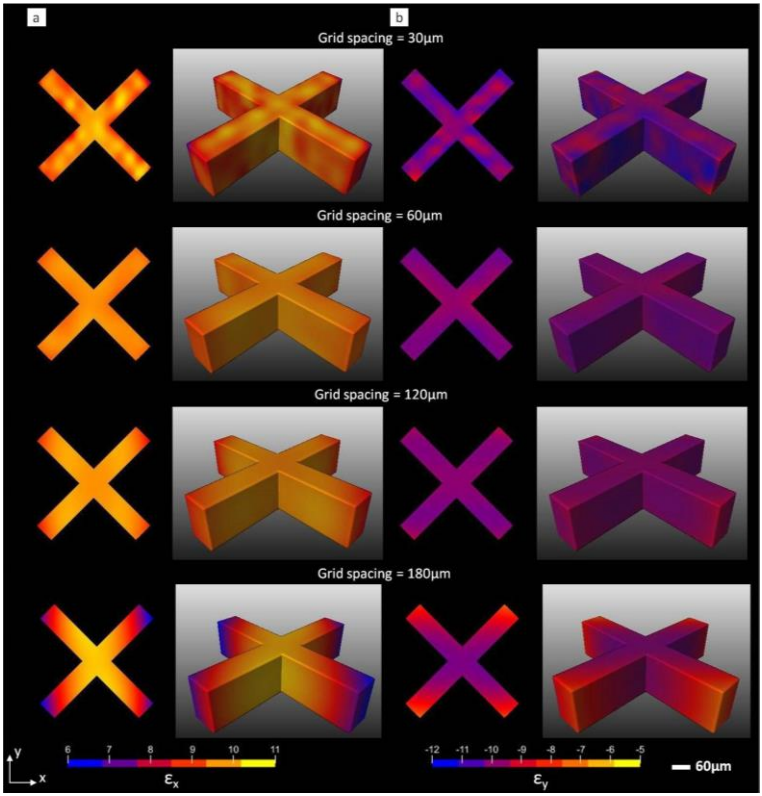

Figure 2. A 2D and 3D visualization of the local strain ε_x (a) and ε_y (b) in the cross-phantom object shrank by about 10% in the y- and stretched by about 10% in the x-direction, calculated using the non-rigid registration approach with different GS: 30, 60, 120 and 180 µm.

The grid spacing influence is a commonly known issue in the image registration process [10]. For instance, it was noted that a reduction of the grid spacing from 64 to 8 mm increases the accuracy of the registration results of clinical MR based medical images of the prostate. However, a further reduction of the grid control points to 4 mm yielded worse results. It was concluded that the finest grid spacing resulted in a too flexible image registration due to a lack of regularization of the B-spline transform [10], i.e. the transformation had too many degrees-of-freedom what resulted in unrealistic deformations.

In this study it was shown that also the strain results calculated the cross-phantom object revealed dependency upon the grid spacing as the strain level and spread increased when refining the grid spacing. However, further refining the grid spacing to 30 µm resulted in a larger error of the mean and mode strain as well as in a larger strain distribution. This implies therefore, that the appropriate grid spacing needs to be defined individually for every tested object depending on the expected complexity of the deformation [10]. This can be done in an iterative process of fine tuning of the distances between the control points, starting from the

relatively coarse GS. However to eliminate the undesirable deformations while the finer GS is applied, an additional regularization term needs to be added to the cost function, which defines the alignment quality of the original and deformed images [10].

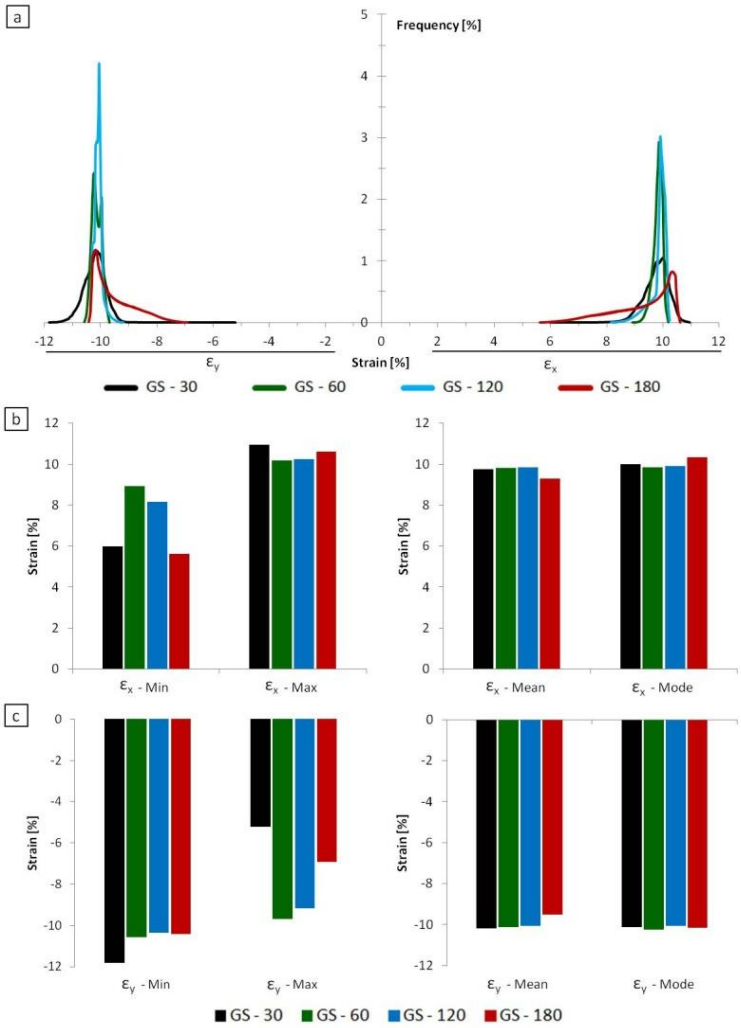

Figure 3. A local distribution of the ε_x and ε_y strain (a) and the minimum, maximum, mean and mode of the ε_x (b) and ε_y (c) strain of the cross-phantom object shrank by about 10% in the y- and stretched by about 10% in the x-direction , calculated using the non-rigid registration approach with different GS: 30, 60, 120 and 180 µm.

Pixel matching test

Figure 4 shows a typical cross-section of a selected basic unit cell from a Ti6Al4V sample compressed until UCS at different steps of the registration process. The reference image of the non-compressed sample is shown in Figure 4a. The global deformation of the beam network (Figure 4b), caused by compressive loading until the UCS, shows bending of a single beam can be observed. The non-rigid registration resulted in a back-deformed image of the tested sample (Figure 4c). Visual observation indicates a reliable registration non-deformed and deformed images, as the initial structure shape was retrieved from the µCT images of the compressed samples using the non-rigid registration approach.

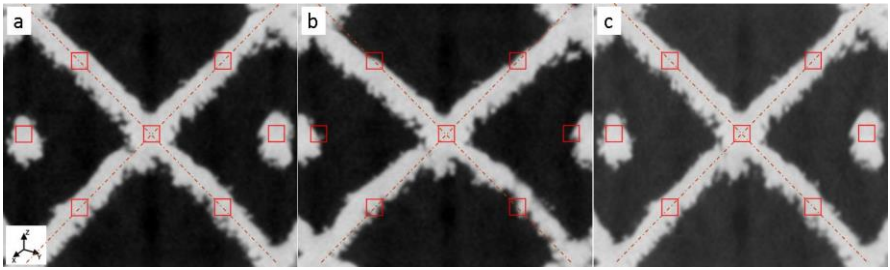

Figure 4. A typical high resolution µCT cross-sectional image of a single unit cell of a Ti6Al4V porous structure: a) before compression, b) compressed until UCS failure and c) the back-registered image of the compressed unit. The red rectangles, with dimensions 100x100 µm, were added to the images for better visual recognition of the structure deformation and the results of the registration process. Compressive loading was applied along the Z-direction.

Furthermore, the results of the pixel matching test confirmed a high accuracy of the registration process. In Table 1, the pixel matching results are presented indicating that the registration quality, observed for the Ti6Al4V porous structure, was dependent on the grid spacing (GS) of the B-spline control points. However, it was shown that the best registration was obtained using a grid spacing of 100µm (lowest pixel match error) thus, the GS 100µm was chosen for further experiments.

Table 1. Positive and negative pixel matching obtained, using different grid spacing from 100 till 800 µm, for Ti6Al4V porous structure compressed until the ultimate compressive strain (UCS).

Grid spacing	Positive pixel match	Negative negative match
[µm]	[%]	[%]
100	99.5	0.4
200	99.4	0.6
300	98.9	0.9
400	97.8	2.0
500	97.8	2.0
600	97.5	2.3
700	96.2	3.4
800	96.8	2.9

Strain mapping analysis of the Ti6Al4V open porous structures

3D visualizations of the central and side plane of a typical sample before and after the different steps of compression (Fig. 5), show a progressive deformation of the interconnected beams. It can be observed that some beams undergo a larger local deformation, which eventually leads to their extreme deformation (at failure). A magnification of a beam connected to the central node (Figure 6a) shows increasing bending with increasing compressive loading. The local strain maps, computed at UCS for the same beam, revealed tensile deformations at the top and compressive deformation at the bottom of the beam (Figure 6b). This corresponds to the bending mechanism of a beam, where the outer side of the beam is stretched while the inner part is compressed.

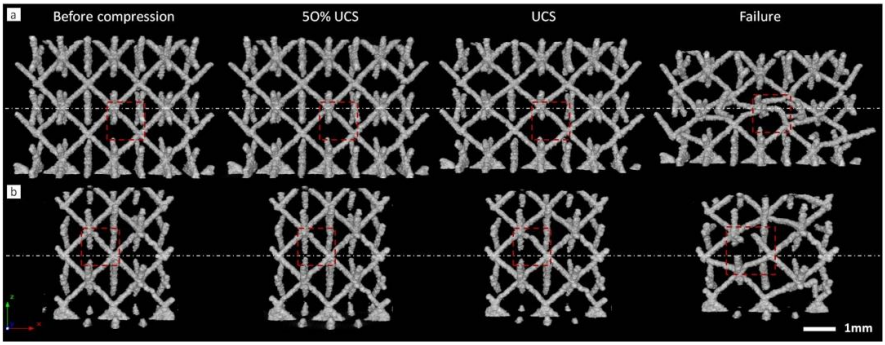

Figure 5. 3D visualization of the beams network, extracted from the centre plane (a) and side plane (b) of the sample before and after all steps of the compression.

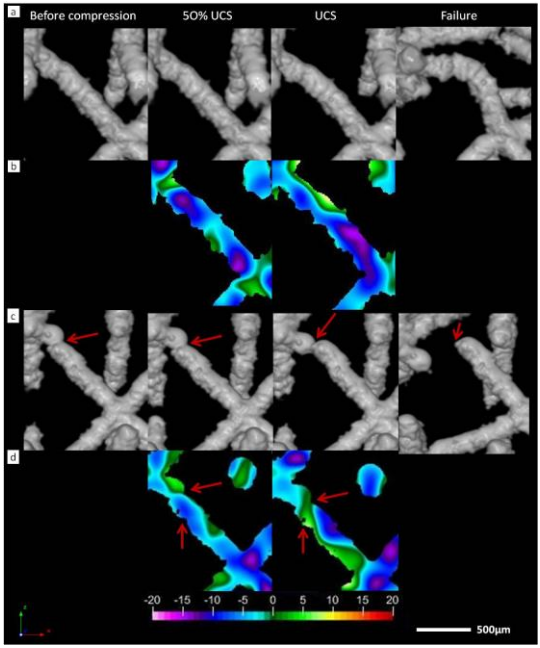

Figure 6. a) and c) magnified 3D images of a single beam marked with red rectangles in figures 5a and 5b respectively and b) and d) 2D maps of the volumetric strain generated for the beam in a) and b) respectively at 50%UCS and at UCS.

Figure 6b presents a beam located at the scaffold side showing clearly its progressive deformation leading eventually to the failure. It can be observed that at the failure step, the mentioned beam was eventually disconnected from the node and displaced in space. However, one can noticed that the strain maps generated, at the compression step-2 (UCS) (Figure 6d) for that beam revealed the tensile strain along the beam bottom section and in the beam section where beam failure occurred. This indicates that the local strain maps generated in this study for the Ti6Al4V porous structure correspond to the real structure deformation that is observed in the µCT images. It is also important to underline that the beam failure (Figure 6c) occurred in the place (marked with red arrow in Figure 6c) where a beam thickness imperfection was seen in the µCT images before compression. This can indicate that that structure thickness variations introduced during SLM production step of Ti6Al4V porous structures can affect the mechanical properties due to increased strain concentrations at these beam imperfections during compression.

Conclusion

In this study the potential and the limitations of the non-rigid image registration approach as a tool for the local strain analysis was assessed. Experiments with the phantom object confirmed the potential of the proposed approach for the local strain analysis as the computed strain corresponded with the deformation artificially applied to the tested object. However, the obtained strain values showed dependency upon the applied grid spacing of the B-spline transformation, due to the unrealistic deformations introduced during the image registration process. This implies that an additional regularization term needs to be added to the cost function in order to eliminate the undesirable deformations.

It was also shown that the strain computed for Ti6Al4V porous structures corresponded well with the real deformation observed visually in the µCT images. This indicates that µCT based strain mapping, performed by combining in-situ loading, µCT imaging and non-rigid image registration of the µCT images, provides a valuable tool to identify and analyze the critical sections in the porous structure having a higher strain concentration. However, further development of the proposed tool is required, in order to optimize the image registration process.

References:

1. Gibson, L.J. et al. “Cellular solids: Structure and Properties”. Cambridge University Press, Cambridge, p. 189-195, 1997.
2. Ohgaki, T. et al.”In situ observations of compressive behaviour of aluminium foams by local tomography using high-resolution X-rays”. Philosophical Magazine, 86(28): p. 4417-4438, 2006.
3. Bay, B.K. et al. “Digital volume correlation: three-dimensional strain mapping using x-ray tomography”. Exp. Mech., 39: p. 217-226, 1999.
4. Liu, L. and Morgan, E.F., “Accuracy and precision of digital volume correlation in quantifying displacements and strains in trabecular bone”. J Biomech, 40: p. 3516-3520, 2007.
5. Lenior, N. et al. “Volumetric digital image correlation applied to x-ray microtomography images from triaxial compression tests on argillaceous rock”. Strain, 43: p. 193-205, 2007.
6. Jandejsek, I. et al. “Precise strain measurement in complex materials using Digital Volumetric Correlation and time lapse micro-CT data”. Procedia Eng., 10: p. 1730-1735, 2011.
7. Kerckhofs, G., et al. “Novel micro-CT-based local strain mapping tool to characterize the failure modes of bone tissue engineering scaffolds”. Skyscan User Meeting, 2009.

8. Maes, F. et al. “Medical image registration using mutual information”. Proceedings of the IEEE, 91(10): p. 1699-1722, 2003.
9. Pyka, G. et al. “Surface roughness and morphology customization of additive manufactured open porous Ti6Al4V structures”. Materials, 6, 4737-4757, 2013.
10. Klein S, et al. “Elastix: a toolbox for intensity-based medical image registration”. IEEE Trans Med Imaging, 29(1): p. 196 – 205, 2010.
11. Loeckx D, et al. “Non-rigid image registration using free-form deformations with a local rigidity constraint”. Medical Image Computing and Computer-Assisted Intervention - Miccai Pt 1, Proceedings, 2004. 3216: p. 639-646, 2004.